PAPER • **OPEN ACCESS**

On Unsteady Flow Analysis of a Round Spike Blunt Nose Afterbody in Mach 6 Flow

To cite this article: A Vashishtha and S Khurana 2021 *IOP Conf. Ser.: Mater. Sci. Eng.* **1024** 012017

On Unsteady Flow Analysis of a Round Spike Blunt Nose Afterbody in Mach 6 Flow

A Vashishtha[1*] and S Khurana[2*]

[1]Department of Aerospace Mechanical & Electrical Engineering, Institute of Technology Carlow, Ireland R93 V960
[2]Department of Mechanical Engineering, BITS Pilani Dubai Campus, Dubai, 345055, UAE
[*]Joint First Authors

Abstract. An aerospike, in front of a blunt body, has largely been deemed as a key passive control device for effectively reducing the wave drag and aerodynamic heating associated with high-speed flows. In addition, it has been reported that the presence of a spike brings in unsteadiness in the form of oscillation and pulsation to the flow characteristics. Past researchers, having investigated mainly the aerothermodynamic coefficients, have hinted towards the suppressing of such oscillations with the use of a round nose spike over a sharp spike, though a thorough and a concrete result is yet to be established together with offering a detailed explanation of the flow physics and its dependence on the spike's geometric characteristics (spike-length to afterbody-diameter ratio, L/D). Numerical investigation has been carried out using axisymmetric Navier-Stokes laminar flow solver at hypersonic Mach number of 6.0. A round-tip spike with a flat face cylindrical afterbody have been simulated for spike length ratios of $L/D = 0.5 - 2.0$, with spike diameter to -afterbody diameter (d/D) of 0.1. The behavior and subsequent control of flow pulsation for a round (hemispherical) spike with varying L/D-ratio has been established.

Keywords: Hypersonic, CFD, unsteadiness, spike, drag control

1. Introduction

A forward-facing spike has largely and unanimously been identified and established as a passive flow control technique to render the strong pressure envelope at the nose in high-speed to become weaker, thereby resulting in reduced pressure over the nose, as a consequence of vortices positioned at the root end, leading to reduction in heat transfer and drag [1]. These key advantages, on the other hand, are challenged by the instability brought in the flow with the presence of a protruding surface, by producing an unbalanced normal component of force and the flow separation caused, and in turn oscillations which would produce adverse moments along the surface of the body in consideration, and in some cases could also have a negative effect on the drag reduction.

Previous researchers [2-3] have identified different types of unsteadiness in front of various spiked blunt noses in hypersonic flows. Further, Kenworthy et al.[4] and Feszty et al. [5] have experimentally and numerically studied the driving mechanism of two distinct spike-induced unsteady flow modes as oscillation and pulsation. The oscillation flow mode is characterized by the foreshock shape change between a convex shape and a concave one, whereas the shock system changes dramatically in the pulsation flow mode. Further, Feszty et al. [6] have explained new mechanism of pulsations by numerical simulation method at Mach number 2.21 and conical tipped spike with $L/D = 1.0$. And Feszty et al. [7] have confirmed about the mechanism of oscillatory mode fluctuations at supersonic and

hypersonic Mach numbers for longer spike length. Khurana et al. [8-9] have studied the flow visualization in a water channel for spiked, conical, and hemispherical tip of spikes at various Reynolds number and analyzed the effectiveness of different shapes analogically for hypersonic applications. Khurana et al. [10] extended the studies of aerospikes to lifting-body configurations in Mach 7 flow and proclaimed the presence of a normal force component bringing in instability for the structure. Kalimuthu et al. [11] have studied the effectiveness of conical, hemispherical, and flat tips of different spikes of length 0.5 to 2.0 for hemispherical-cylinder blunt nose and found the maximum drag reduction of 78% for L/D = 2.0. However, there is no unsteadiness found associated with spiked body on hemispherical-cylinder blunt nose.

Table 1 summarizes the previous studies [11-18] conducted on investigating the effects of the presence of a hemispherical (round) tipped aerospike in front of a blunt afterbody in hypersonic flow. While all the studies primarily investigated the effects of varying (L/D)-ratio on aerodynamic forces, they provided limited insight into the unsteadiness generated around the body. Researchers [11-13] also studied and quantified the effects associated with the changes in angle of attack. Sahoo et al. [19] investigated the effects of geometrical parameters of spike on a hemispherical afterbody in a supersonic flow of Mach 2. The intensity of shock-related unsteadiness was examined, and its characteristics were explained together with concluding the superiority of a hemispherical spike in reducing the aerodynamic drag as well as unsteadiness.

Table 1. Summary of previous studies focussed on hemispherical (round) tip spike

Reference	Mach No.	Angle of Attack (deg.)	Afterbody	Spike Length, L/D	Spike Diameter, d/D	Investigation Type
Kalimuthu et al. [11]	6	0 – 8	Hemispherical	0.5 – 2	0.1	Experimental
Motoyama et al. [12]	7	0 – 8	Hemispherical	0.5, 1	0.1	Experimental
Kalimuthu et al. [13]	6	> 0	Hemispherical	1.5, 2	0.1	Experimental
Gauer et al. [14]	5, 7, 10	0	Blunt Cone	1 – 4	0.1	Numerical
Mansour et al. [15]	6	0	Hemispherical	1.5	0.1	Numerical
Qin et al. [16]	5	0	Hemispherical	1	0.05	Numerical
Li et al. [17]	5	0	Hemispherical	0.5 – 2	0.1	Numerical
Mehta [18]	2 – 6	0	Blunt Cone & Hemispherical	0.5 – 2	0.1	Numerical
Sahoo et al. [19]	2	0	Hemispherical	0.5 – 2	0.06, 0.12, 0.18	Experimental + Numerical
Current Research	6	0	Flat-faced	0.5 – 2	0.1	Numerical

The pulsation unsteadiness has exhibited the features of higher amplitude and non-symmetry in the flow-field, which may lead to unsteady loads of high amplitude on front face of afterbody. In the absence of enough research focusing on a spiked body unsteadiness in hypersonic flow, the current study is aimed at performing a numerical investigation with the objective of studying the effect of varying spike length (L/D-ratio) on pulsation unsteadiness (oscillation characteristics of inflation and collapse of shock waves) in front of a flat afterbody in Mach 6 flow, and subsequently understanding the characteristics of shock interaction and its location on the body corner. A round nose spike has been chosen for this study.

2. Geometric Consideration

A round-tipped spike in front of flat-face blunt nose body has been investigated for different lengths (L/D = 0.5–2.0), as shown in figure 1. Here, L is the spike length and D is the maximum cross-sectional diameter of the base blunt nose (in current study, D = 40 mm). The spike root diameter (denoted as d) has been fixed at d/D = 0.1 in reference to similar previous studies [11-15,17,18]. The appropriate comparisons have been made with a no-spike body to characterize the pulsation behaviour and its dependence on the length of the spike.

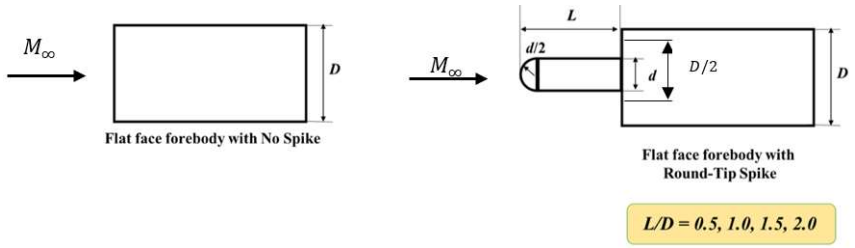

Figure 1. Geometric parameters

3. Numerical Method

In the current study, two-dimensional structured grids have been generated in the computational domain for a flat-face cylindrical base body with a round nose tip. The computations are performed by solving unsteady axisymmetric Navier-Stokes equations for laminar compressible flows. The spatial inviscid fluxes are evaluated by Lious all-speed AUSM (Advection Upstream Splitting Method) + up scheme [20] with upwind biased third order MUSCL (monotonic upstream-centered scheme for conservative laws) interpolation, while viscous fluxes, as well as source terms (because of axisymmetry), have been evaluated using the second order central difference scheme. The third order TVD Runge - Kutta Method [21] was employed for time integration.

Table 2. Test Conditions

VKI Hypersonic Tunnel Conditions	
Mach number	6.0
Stagnation Pressure (P_0)	400 kPa
Stagnation Temperature (T_0)	500 K
Reference Length	40 mm
Adiabatic Wall Temperature	300 K
Reynolds Number	0.134 x 10^6
Simulation Physical Time	4 ms

3.1. Computational Domain

Figure 2(a) and 2(b) shows the structured grid generated using elliptic grid generation method for a no-spike and a round-tip spike (L/D = 2.0) respectively both in front of flat-face cylindrical aftebody. For all the cases, the domain is used with 151x101 grid points after grid independence test.

3.2. Boundary and Initial Conditions

The boundary condition at the inlet section given according to flow condition used by Feszty [5] of hypersonic flow condition Mach 6.0. However, the reference length or diameter of blunt nose have been used as 40 mm for current study as shown in table 2. At the wall, *no-slip* boundary condition along with isothermal constant wall temperature 300 K is assumed. The outlet is treated as supersonic outlet with first order interpolation of fluxes from the inner domain. The flow is initiated with low velocity around

the spike and blunt nose and considered to have an impulse start. All the computations are performed for 4 ms time duration.

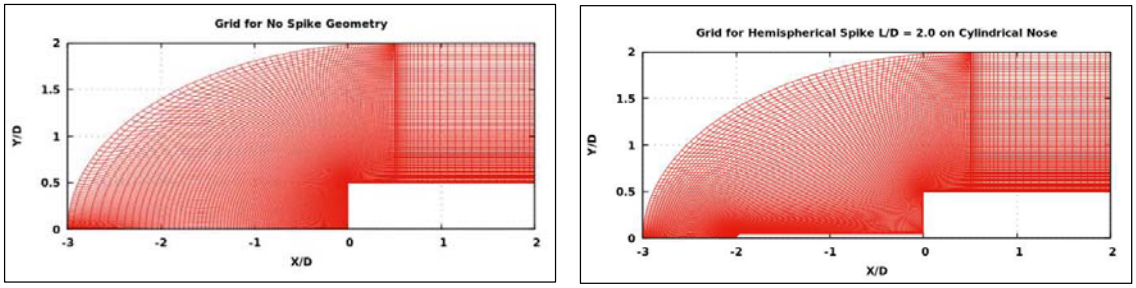

(a) **(b)**

Figure 2 (a) Grid for no-spike geometry, (b) Grid for round spike (L/D=2.0)

3.3. Code Validation / Grid Independence

In order to evaluate performance of current code, the simulations are performed for round tipped spike for flat cylindrical blunt nose, similar to Feszty [5] for hypersonic flow condition, where the reference diameter (D) is 46 mm and spike diameter d = 0.065D. The computation grids are generated with maximum dimensions of 4mm, 2mm and 1 mm as coarse (76 x 51), medium (151 x 101) and fine (301 x 201) grid, respectively. The computations are performed for Mach Number 6.0 and Reynolds Number 0.15 million. Figure 3 shows the results obtained from the simulations for 4 ms time-interval for all three grid configurations. Figure 3(a) shows the non-dimensionalized pressure ($P/\rho V^2$) variation at Y location D/2 on the front face, and figure 3(b) shows the variation of drag coefficient with time. The various phases of pulsating flow cycle (collapse, withhold and inflate) have been observed for all three grid configurations. During the initial cycles of pulsating flow, it can be seen that for all three grid sizes, the pressure and drag coefficients have been behaving in similar manner, while after 2 ms, there is a slight phase difference between the pulsation cycles. However, variation in pressure and drag coefficient have almost similar amplitude and least difference in phase of time variation for medium and fine grid. Hence, 2 mm medium grid size have been used in all the further studies. The non-dimensional Strouhal Number, which can be defined as $\left(S_R = \frac{fD}{V_\infty} \right)$, have been found as 0.114 after 2 ms, and non-dimensional pressure fluctuations have been in the range of 0 to 2 for 2mm grid case, which can be considered close to Feszty et al.[5] results, and the accuracy of current simulations methods can be considered adequate for the current comparative study.

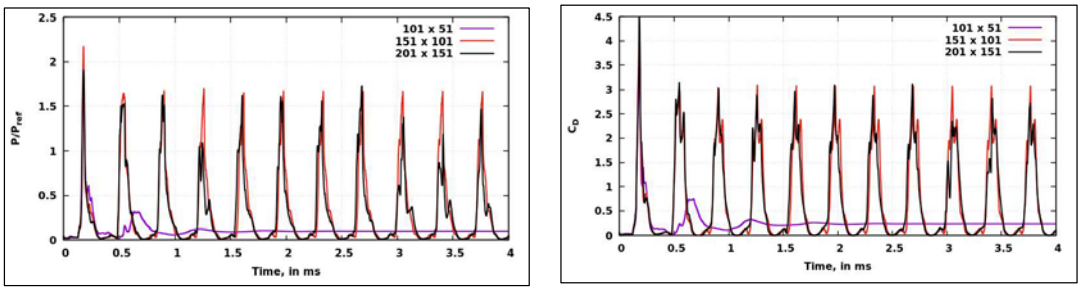

(a) **(b)**

Figure 3. **(a)** Pressure at front face location D/2, and **(b)** Drag Coefficient variation with time for different grids (both for round spike body L/D=2.0)

4. Results and Discussions

The numerical computations have been performed for a reference diameter, D = 40 mm, spike diameter d/D = 0.1 and spike length L/D = 2. The freestream conditions are also same for all the studies as Mach number 6 and Reynolds number 0.134 million. The study has been performed to ascertain the effect of spike length on the flow unsteadiness in front of flat-faced afterbody. The results are presented and discussed by plotting Mach number contours, drag coefficient variation with time as well as the pressure calculated at $D/2$ and D locations.

4.1 Mach Number

The no-spike body demonstrates the absence of any pulsation existing in the flow. Figure 4 shows the Mach number contours at the end of inflation phase, and figure 5 for the collapse phases, respectively for L/D=0.5, 1.0, 1.5 and 2.0. For all the spike cases, a vertical normal shock exists in front of spike nose. At the end of collapse phase, the triple point of forebody and afterbody shocks is farther from the front face of blunt nose resulting optimum pressure. From these simulations, it is understood that after the end of collapse phase, the inflation phase is caused by sharp corner at the flat front phase, which requires a small build up in pressure for escaping the mass build up in the zone between spike and front face. A slight pressure gradient near the corner may reduce the shock unsteadiness.

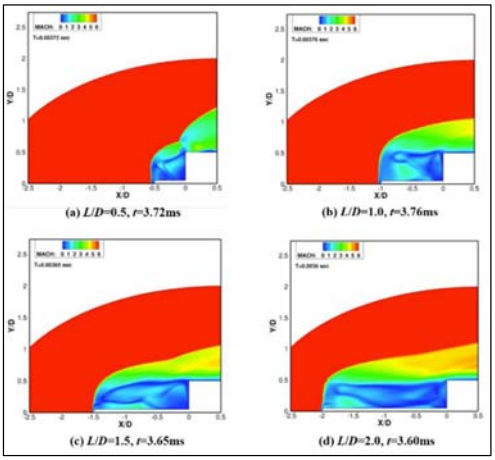

Figure 4. Mach number contours for spiked body demonstrating *inflation* with variation (L/D)-ratio

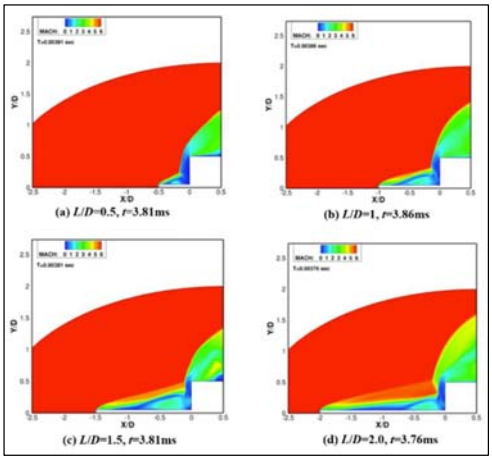

Figure 5. Mach number contours for spiked body demonstrating *collapse* with variation (L/D)-ratio

From figure 4(a)-(d), it can be inferred that with the increase in the length of the spike, the shock after having inflated to the maximum extent, demonstrates a curved profile owing to the suction created at the spike root. Observing figure 5(a)-(d) highlights the movement of shock during the collapse phase of oscillation, signifying that with increase in the length of the spike, the reattachment location moves away to from the spike root towards the corner of the flat-face body. The forebody bow shock interacts with afterbody bow shock far from the corner in Edney Type V interaction [22] and shear layer stabilize near the corner. Comparing the time stamps of corresponding figures 4 and 5 for similar L/D-ratio, it can be seen that the duration of withhold phase of shock (duration between collapse and inflation phases), increases with increase in spike length.

4.2 Drag Coefficient

Figure 6 shows the drag coefficient characteristics for a no-spike body and round-spike body with varying lengths. It can be observed that no-spike body (L/D=0) marks a constant value demonstrating the associated steady flow. For the spiked bodies, the peak shows completed collapse, while decrease in drag shows the inflation process and the minima shows the withhold process of the shock wave. It can also be observed that the time duration for withhold phase increases with increase in spike length.

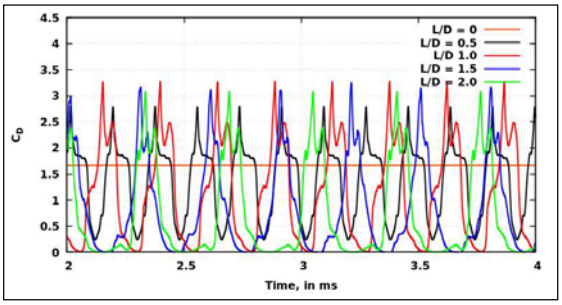

Figure 6. Drag coefficient

4.3 Pressure Characteristics

Figure 7 shows the normalized pressure characteristics, and its comparison between no-spike and spiked bodies (with varying length), calculated at two locations on the front face, (a) at $D/2$, and (b) at the corner location D. The instantaneous movement of shock wave is clear from figure 7(a), and a clear depiction of two separate peaks in figure 7(b) for spiked bodies, as the pressure pulse moves past through the corner of the flat-faced forebody two times.

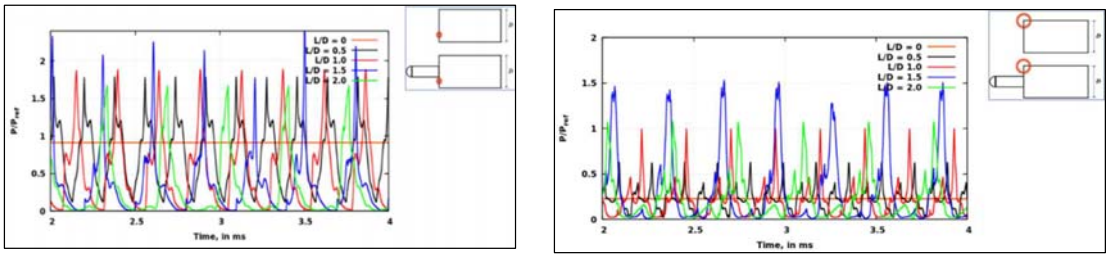

(a) At front face location (D/2) *(b) At front face location (D)*

Figure 7. Non-dimensional pressure characteristics variations with (L/D)-ratio

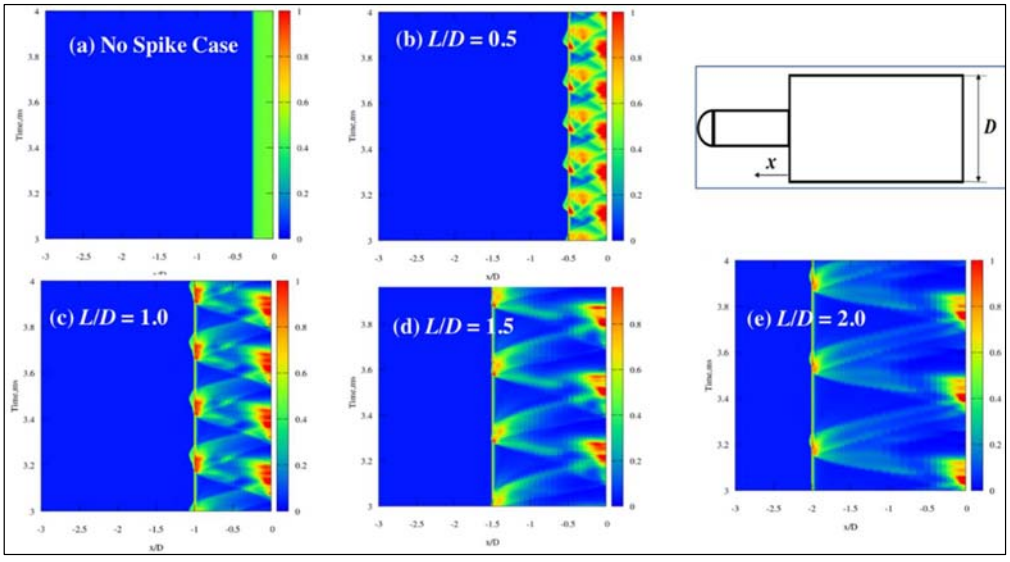

Figure 8. x-t for Stagnation Line and Spike Wall (P/P_{ref})

Figure 8 shows the contours of normalized pressure characteristics (P/P_{ref}) depicted on stagnation line in front of the afterbody (with and without spikes), and on the spike nose wall. It can be easily observed

that with the increase in length of the spike, the number of peak pressure zone reduces, also signifying the reduction in the oscillation frequency. High pressure zones are observed near the spike tip as well as at the frontal base of the body, however there is a slight phase delay in high pressure zones at both the locations, but remains same during multiple cycle for particular spike.

4.4 Fundamental Frequency

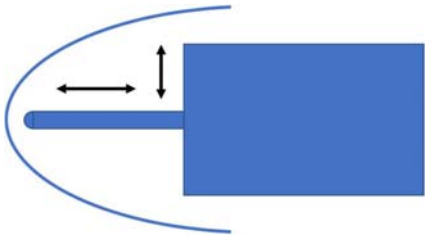

Figure 9. Fundamental frequency

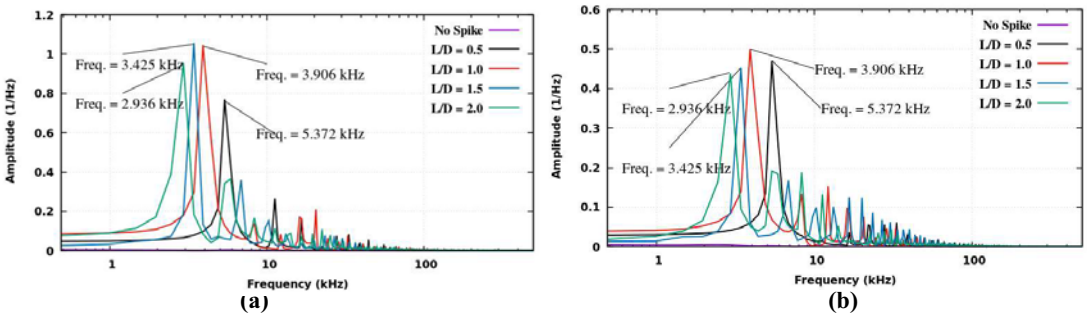

Figure 10. Fundamental frequency variation with (*L*/*D*)-ratio, **(a)** Drag coefficient oscillations, and (**b**) Pressure oscillations at *D*/2 location

Table 3. Frequency Analysis

Cases	C_D (Time averaged) ± SD	St	Frequency from FFT (kHz)	Axial Frequency (kHz)	Traverse Frequency (kHz)
No Spike	1.665± 0.009	NA	NA	NA	NA
L/*D* = 0.5	1.361± 0.730	0.114	5.372	11.207	5.803
L/*D* = 1.0	1.129± 0.962	0.166	3.906	5.513	5.803
L/*D* = 1.5	0.811±0.861	0.221	3.452	3.675	5.803
L/*D* = 2.0	0.695±0.900	0.250	2.936	2.757	5.803

In order to understand the unsteadiness in front of a spiked body through characteristics oscillation frequency, a spiked body can be modelled as open pipe in order to evaluate the axial and the transverse motions of the flow field (shock). The characteristic length for axial frequency can be assumed as length of spike, however the characteristic length for transverse frequency can be assumes as (*D*–*d*)/2, as shown in figure 9. The fundamental axial and transverse frequency can be given by $f = n\frac{V_a}{2L}$, here V_a is speed of sound after the shock, L is characteristic length, n is number of modes. Strouhal number is calculated from the calculated frequency from FFT as $St = \frac{fL}{V_\infty}$, here V_∞ is freestream velocity and L is characteristic length of spike and f is frequency from FFT. Table 3 summarizes the evaluated characteristics for the different test cases. The time-averaged drag with standard deviation is tabulated

along with measured Strouhal number. The axial and traverse frequencies have been compared with measured frequency from FFT. With increase in spike length, the standard deviation in drag coefficient increases, however, the time-averaged drag coefficient decreases with increase in length of spike. The Strouhal number also increases with increase in spike length. The computed frequency from FFT have shown decreasing trend as increase in spike length as shown in figure 10(a)-(b). When the measured frequency is compared with the theoretical axial and transverse frequency, it was observed that the longer spike lengths are dominated by axial frequency motion and the shorter spikes are dominated by traverse frequency motion.

5 Conclusions

In the current study, the unsteady behaviour of flow field in front of round-tip spikes of length L/D = 0.5-2.0, attached to a flat-faced cylindrical afterbody, have been investigated using axisymmetric numerical simulations. It is found that forebody shock of hemispherical tipped spike interacts with afterbody shock in different manners for different spike lengths and consequently results in different pulsation frequencies. The time-averaged drag coefficient reduces with the increase in spike length, while the amplitude of drag unsteadiness also increases. The computed frequencies of pulsation are close to the fundamental transverse frequency for smaller spike length, while it is close to the axial fundamental frequencies for longer spike length. Although, tip of the spike may affect how the forebody bow-shock at tip may interact with the afterbody shock, but overall frequencies of unsteadiness mainly depend on two geometrical features in spiked blunt body system. It may be further required to provide additional flow control method to use the spike effectively for its drag reduction ability.

6 References

[1] Ahmed M Y M and Qin N 2019 *Prog. Aerosp. Sciences* **112** 100585.
[2] Maull D J 1960 *Jl.* Fluid Mech. 8 **4** 584-592.
[3] Wood C J 1961 *Jl.* Fluid Mech. 12 **4** 614-624.
[4] Kenworthy M A 1978 *Ph.D. Thesis* Virginia Polytechnic Institute.
[5] Feszty D, Badcock K J, Richards B E and Woodgate MA 2000 *Shock Waves* 10 **5** 323-331.
[6] Feszty D, Badcock K J, Richards B E 2004 *AIAA J.* 42 **1** 95-106.
[7] Feszty D, Badcock K J, Richards B E 2004 *AIAA J.* 42 **1** 107-113.
[8] Khurana S, Suzuki K and Rathakrishnan E 2016 *Modern Physics Letters B* 30 **30** 1650362.
[9] Khurana S, Suzuki K and Rathakrishnan E 2017 *Int. Review Aerosp. Engg. J.* 10 **4** 189-195.
[10] Khurana S and Suzuki K 2012 *Trans. JSASS Aerospace Tech. Japan* **10** 15-24.
[11] Kalimuthu R, Mehta R C and Rathakrishnan E 2017 *The Aeronaut. J.* 121 **1245** 1711-1732.
[12] Motoyama N, Mihara K, Miyajima R, Watanuki T and Kubota H 2001 AIAA/NAL-NASDA-ISAS 10th International Space Planes and Hypersonic Systems and Technologies Conference Kyoto, Japan.
[13] Kalimuthu E and Rathakrishnan E (2008) 44th AIAA/ASME/SAE/ASEE Joint Propulsion Conference & Exhibit, Hartford, USA.
[14] Gauer M and Paull A 2008 *J. Spacecraft Rockets* 45 **3** 459-471.
[15] Mansour K and Khorsandi 2014 *Acta Astronautica* 99 92-98.
[16] Qin Q, Xu J and Guo S 2017 *Acta Astronautica* 132 230-242.
[17] Li Z, Sun C, Xia X and Li X, 2018 *J. Aerosp. Eng.* 31 **6** 04018083.
[18] Mehta R C 2018 *Heat Transfer - Models, Methods and Applications* (IntechOpen) pp 175-198.
[19] Sahoo D, Karthick S K, Das S and Cohen J 2020 *AIAA J.* 58 **8** 1-18.
[20] Liou M S 2006 *J. Comp. Physics* 214 **1** 137-170.
[21] Shu C W and Osher S 1988 *J. Comp. Physics* **77** 439-471.
[22] Edney B E 1968 *AIAA J.* **6** 15-21.